

EFFICIENT SOLUTIONS OF METAMATERIAL PROBLEMS USING A LOW-FREQUENCY MULTILEVEL FAST MULTIPOLE ALGORITHM

Ö. Ergül

Department of Mathematics and Statistics
University of Strathclyde
Glasgow, UK

L. Gürel [†]

Department of Electrical and Electronics Engineering
Bilkent University
Bilkent, Ankara, Turkey

Abstract—We present fast and accurate solutions of electromagnetics problems involving realistic metamaterial structures using a low-frequency multilevel fast multipole algorithm (LF-MLFMA). Accelerating iterative solutions using robust preconditioning techniques may not be sufficient to reduce the overall processing time when the ordinary high-frequency MLFMA is applied to metamaterial problems. The major bottleneck, i.e., the low-frequency breakdown, should be eliminated for efficient solutions. We show that the combination of an LF-MLFMA implementation based on the multipole expansion with the sparse-approximate-inverse preconditioner enables efficient and accurate analysis of realistic metamaterial structures. Using the robust LF-MLFMA implementation, we demonstrate how the transmission properties of metamaterial walls can be enhanced with randomly-oriented unit cells.

Received 11 July 2010, Accepted 7 August 2010, Scheduled 10 September 2010

Corresponding author: Ö. Ergül (ozgur.ergul@strath.ac.uk).

[†] Also with Computational Electromagnetics Research Center (BiLCEM), Bilkent University, Bilkent, Ankara, Turkey.

1. INTRODUCTION

Metamaterials — artificial structures constructed by periodically arranging small unit cells — have become very popular due to their useful electromagnetic properties, which cannot be obtained with natural materials [1–4, 27–32]. Numerical solutions of metamaterial problems are also important since they can provide essential information on novel structures without their actual realizations [5]. In many cases, the accuracy of numerical solutions is critical for reliable analysis, and full-wave solutions are necessary rather than homogenization techniques. However, there are two major difficulties encountered in solving metamaterial structures conventionally. First, metamaterials exhibit resonances, leading to ill-conditioned problems that are difficult to solve [6]. As a remedy, problems can be reformulated in more stable ways [7], or in the case of iterative solvers, robust preconditioning techniques can be used to externally improve the conditioning of the problems [8]. Second, metamaterials usually involve small details with respect to wavelength, whereas their overall sizes are in the orders of wavelength. Hence, fast solvers designed for high-frequency applications may fail to analyze metamaterials efficiently and accurately, and low-frequency algorithms are required to improve the solutions.

The multilevel fast multipole algorithm (MLFMA) [9, 10] is a fast and accurate method for solving electromagnetics problems. This algorithm can perform the matrix-vector multiplications required by iterative techniques in $\mathcal{O}(N \log N)$ time using $\mathcal{O}(N \log N)$ memory for an $N \times N$ dense matrix equation. Therefore, it is suitable for the analysis of realistic metamaterials involving hundreds of unit cells and discretized with large numbers of unknowns. Without assuming any periodicity and regularity, MLFMA is able to analyze metamaterials involving randomly oriented, defected, and mixed unit cells [8, 11]. Unfortunately, the ordinary high-frequency MLFMA (HF-MLFMA) suffers from a well-known low-frequency breakdown problem. Specifically, subdomains in HF-MLFMA cannot be very small compared to the wavelength. This is a serious problem for metamaterial structures, which usually involve small details that must be discretized with small elements compared to the wavelength.

When HF-MLFMA is applied to metamaterial structures, the lowest-level subdomains may involve many discretization elements. This increases the processing time and memory required for near-field interactions that must be calculated directly, and the efficiency of the implementation may drop significantly. As the near-field matrix becomes less sparse, the overall complexity of the MLFMA

implementation may be higher than $\mathcal{O}(N \log N)$, and this would not be desirable at all. Hence, low-frequency implementations of this algorithm are required to improve the solutions, to keep the computational complexity low, and to enable the solution of larger problems with limited computational resources.

Stabilization of MLFMA for low-frequency applications has attracted the interest of many researchers, leading to development of diverse approaches to solve the low-frequency breakdown problem [12–23]. In one approach, spectral representation of the Green's function is used so that electromagnetic waves are divided into propagating and evanescent parts [12–15]. Then, the interactions between small subdomains separated by short distances can be calculated accurately using the evanescent waves. Although this approach leads to very accurate implementations that are stable in low-frequency regimes, evanescent waves require direction-dependent translation procedures that may reduce the efficiency. The problem of direction dependency is solved in another approach [15, 16], so called uniform MLFMA, where the Green's function is represented in a novel way using a modified integration contour. Unfortunately, the accuracy of the resulting implementation is not totally controllable, whereas error controllability is an essential requirement for highly-accurate computations. A third and more rigorous approach is based on the multipole representation of electromagnetic waves [17–23]. The Green's function is factorized with a multipole series, but the multipoles are not converted into plane waves for diagonalization. Without the diagonalization, an LF-MLFMA implementation based on the multipole representation does not suffer from the low-frequency breakdown. In addition to its controllable accuracy, multipoles do not require direction-dependent operations. Furthermore, it is relatively easy to construct a broadband implementation of MLFMA [22, 23], where plane-wave and multipole representations are used at higher and lower levels, respectively, of the same tree structure.

In this paper, we present fast and accurate solutions of metamaterial problems using a low-frequency MLFMA (LF-MLFMA) based on the multipole representation [17–23]. We show that, by combining LF-MLFMA with a robust preconditioner, such as the sparse-approximate-inverse (SAI) preconditioner [24, 25], complicated metamaterial problems can be solved efficiently and accurately. The developed LF-MLFMA implementation is employed to demonstrate the enhanced transmission properties of metamaterial structures involving randomly-oriented unit cells.

2. MULTILEVEL FAST MULTIPOLE ALGORITHM

Discretizations of surface integral equations lead to $N \times N$ dense matrix equations in the form of

$$\bar{\mathbf{Z}} \cdot \mathbf{a} = \mathbf{v}, \quad (1)$$

where the matrix elements $\bar{\mathbf{Z}}[m, n]$ for $m, n = 1, 2, \dots, N$ can be interpreted as electromagnetic interactions of discretization elements, i.e., basis and testing functions. The matrix equation (1) can be solved iteratively via a Krylov subspace algorithm, where the required matrix-vector multiplications are performed efficiently by MLFMA. Matrix-vector multiplications are decomposed into two parts as

$$\bar{\mathbf{Z}} \cdot \mathbf{x} = \bar{\mathbf{Z}}_{NF} \cdot \mathbf{x} + \bar{\mathbf{Z}}_{FF} \cdot \mathbf{x}, \quad (2)$$

where near-field interactions denoted by $\bar{\mathbf{Z}}_{NF} \cdot \mathbf{x}$ are performed directly whereas far-field interactions denoted by $\bar{\mathbf{Z}}_{FF} \cdot \mathbf{x}$ are performed efficiently in a group-by-group manner using the factorization of the homogeneous-space Green's function. A multilevel tree structure of L levels is constructed by placing the object in a cubic box and recursively dividing the computational domain into subdomains. Using the tree structure, interactions between distant subdomains are computed efficiently in three stages, namely, aggregation, translation, and disaggregation.

2.1. General Formulation

In the aggregation stage, radiated fields of subdomains are calculated from the bottom of the tree structure to the highest level ($l = L$). At the lowest level,

$$\{\mathbf{S}_R^C, \mathbf{S}_\theta^C, \mathbf{S}_\phi^C, \mathbf{S}_S^C\} = \sum_{n \in C} \mathbf{x}[n] \{\mathbf{S}_R^n, \mathbf{S}_\theta^n, \mathbf{S}_\phi^n, \mathbf{S}_S^n\}, \quad (3)$$

where $\mathbf{x}[n]$ represents coefficients provided by the iterative solver, $\{\mathbf{S}_R^C, \mathbf{S}_\theta^C, \mathbf{S}_\phi^C, \mathbf{S}_S^C\}$ are arrays containing the radiated field of a subdomain C , and $\{\mathbf{S}_R^n, \mathbf{S}_\theta^n, \mathbf{S}_\phi^n, \mathbf{S}_S^n\}$ are arrays containing the radiation pattern of the n th basis function located inside C . In this general form, we consider the scalar potential part (\mathbf{S}_S), in addition to the vector-potential part in spherical coordinates (\mathbf{S}_R , \mathbf{S}_θ , and \mathbf{S}_ϕ). For a subdomain C at level $l > 1$,

$$\{\mathbf{S}_R^C, \mathbf{S}_\theta^C, \mathbf{S}_\phi^C, \mathbf{S}_S^C\} = \sum_{C' \in C} \bar{\beta}_{C' \rightarrow C} \cdot \{\mathbf{S}_R^{C'}, \mathbf{S}_\theta^{C'}, \mathbf{S}_\phi^{C'}, \mathbf{S}_S^{C'}\}, \quad (4)$$

where $\bar{\beta}_{C' \rightarrow C}$ is a matrix representing the shift operation from the center of C' (located inside C) to the center of C .

In the translation stage, radiated fields computed during the aggregation stage are translated into incoming fields. For each subdomain at any level, there are $\mathcal{O}(1)$ subdomains to translate the radiated field to. For a subdomain C at level l ,

$$\{\mathbf{G}_R^C, \mathbf{G}_\theta^C, \mathbf{G}_\phi^C, \mathbf{G}_S^C\} = \sum_{C' \in \mathcal{F}\{C\}} \bar{\alpha}_{C' \rightarrow C} \cdot \{\mathbf{S}_R^{C'}, \mathbf{S}_\theta^{C'}, \mathbf{S}_\phi^{C'}, \mathbf{S}_S^{C'}\}, \quad (5)$$

where $\{\mathbf{G}_R^C, \mathbf{G}_\theta^C, \mathbf{G}_\phi^C, \mathbf{G}_S^C\}$ are arrays containing the incoming field to the center of C , $\mathcal{F}\{C\}$ represents subdomains that are far from C , and $\bar{\alpha}_{C' \rightarrow C}$ is a square translation matrix.

In the disaggregation stage, the total incoming fields at subdomain centers are calculated from the top of the tree structure to the lowest level. For a subdomain C at level $l < L$, the total incoming field can be written as

$$\begin{aligned} \{\mathbf{G}_R^{C,+}, \mathbf{G}_\theta^{C,+}, \mathbf{G}_\phi^{C,+}, \mathbf{G}_S^{C,+}\} &= \{\mathbf{G}_R^C, \mathbf{G}_\theta^C, \mathbf{G}_\phi^C, \mathbf{G}_S^C\} \\ &+ \bar{\beta}_{\mathcal{P}\{C\} \rightarrow C} \cdot \{\mathbf{G}_R^{\mathcal{P}\{C\}}, \mathbf{G}_\theta^{\mathcal{P}\{C\}}, \mathbf{G}_\phi^{\mathcal{P}\{C\}}, \mathbf{G}_S^{\mathcal{P}\{C\}}\}, \end{aligned} \quad (6)$$

where $\mathcal{P}\{C\}$ is the parent subdomain of C , i.e., $C \in \mathcal{P}\{C\}$. We note that

$$\bar{\beta}_{\mathcal{P}\{C\} \rightarrow C} = \bar{\beta}_{C \rightarrow \mathcal{P}\{C\}}^\dagger, \quad (7)$$

where ‘ \dagger ’ represents the transpose complex-conjugate operation. Finally, at the lowest level, incoming fields are received by testing functions as

$$\sum_{n=1}^N \bar{\mathbf{Z}}_{FF}[m, n] \mathbf{x}[n] \propto \mathbf{F}_R^m \cdot \mathbf{G}_R^{C,+} + \mathbf{F}_\theta^m \cdot \mathbf{G}_\theta^{C,+} + \mathbf{F}_\phi^m \cdot \mathbf{G}_\phi^{C,+} + \mathbf{F}_S^m \cdot \mathbf{G}_S^{C,+}, \quad (8)$$

where $m \in C$, and $\{\mathbf{F}_R^m, \mathbf{F}_\theta^m, \mathbf{F}_\phi^m, \mathbf{F}_S^m\}$ are arrays containing the receiving pattern of the m th testing function. In (8), we use proportionality (\propto) instead of equality ($=$), since there is usually a constant factor depending on the definition of the radiation and receiving patterns of the basis and testing functions.

2.2. High-frequency MLFMA

In HF-MLFMA, radiated and incoming fields are represented by plane waves. For level $l = 1, 2, \dots, L$, the number of samples (plane-wave directions) is $S_l = (T_l + 1)^2$, where T_l is the truncation number determined by the excess bandwidth formula [26]. In general, the

truncation number is proportional to the subdomain size as measured by the wavelength. In spherical coordinates, only θ and ϕ components of the vector-potential part are required, since the radial component of the vector potential and the scalar potential cancel each other. Using plane waves, translation matrices are diagonal, and this is an important advantage in terms of efficiency. In addition, shift matrices are sparse when local interpolation methods are used to match different sampling rates of the consecutive levels. We note that, in HF-MLFMA, the receiving operations by the testing functions involve angular integrations. These are represented implicitly by the inner products in (8), whereas the integration weights are embedded into the diagonal translation matrix.

2.3. Low-frequency MLFMA

Alternatively, metamaterial problems can be solved efficiently via LF-MLFMA based on an explicit representation of radiated and incoming fields in terms of multipoles [17–23]. For level $l = 1, 2, \dots, L$, the number of multipoles is $M_l = (T_l + 1)^2$, where T_l is the truncation number. By performing a worst-case analysis, it can be shown that, for subdomains smaller than the wavelength, the truncation number is almost constant and it does not depend on the subdomain size. Hence, even though the shift and translation matrices are dense, LF-MLFMA can be used efficiently to investigate metamaterial structures with dimensions of several wavelengths. In addition, as opposed to HF-MLFMA, the size of subdomains is not restricted, and one can recursively divide the object into subdomains, which can be much smaller than the wavelength. Consequently, LF-MLFMA can be more efficient than HF-MLFMA for metamaterial problems involving dense discretizations.

We emphasize that LF-MLFMA may not be appropriate for very large-scale problems since the multipole representation becomes inefficient for large subdomains. Specifically, the number of multipoles required to represent the radiated and incoming fields grows rapidly for subdomains that are larger than 2λ , where λ is the wavelength. Such subdomains are required for objects larger than 8λ . For those problems, one needs to employ a broadband implementation of MLFMA [22, 23], where HF-MLFMA and LF-MLFMA are used at higher and lower levels, respectively, of the same tree structure. Application of a broadband MLFMA to metamaterial structures will be reported elsewhere.

3. RESULTS

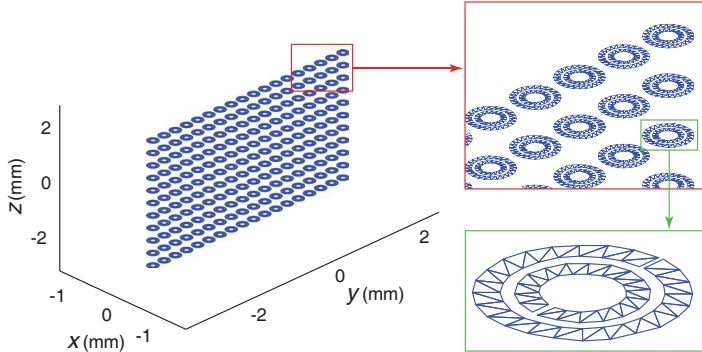


Figure 1. A metamaterial wall involving 18×11 SRRs.

In order to compare HF-MLFMA and LF-MLFMA, we consider scattering problems involving two metamaterial walls constructed by periodically arranging split-ring resonators (SRRs). Fig. 1 depicts a one-layer metamaterial wall involving 18×11 SRRs. A single SRR has dimensions in the order of microns and resonates at about 100 GHz when embedded into a homogeneous host medium with a relative permittivity of 4.8 [3]. The periodicity of SRRs is $262.7 \mu\text{m}$ and $450 \mu\text{m}$ in the y and z directions, respectively. In addition to this one-layer wall, a four-layer metamaterial wall is constructed by stacking four one-layer walls with $262.7 \mu\text{m}$ periodicity in the x direction. Both walls are illuminated by a Hertzian dipole located at $x = 1.2 \text{ mm}$ and oriented in the y direction. For numerical solutions, surfaces are discretized with $\lambda/100$ triangles, where λ is the wavelength in the host medium at 100 GHz. Those dense discretizations are required for the accurate modelling of SRRs. Problems are formulated with the electric-field integral equation (EFIE) discretized with the Rao-Wilton-Glisson (RWG) functions, and matrix equations involving 16,236 and 64,944 unknowns are solved iteratively by the generalized-minimal residual (GMRES) algorithm without restart. The maximum number of iterations is set to 4000. Matrix-vector multiplications are performed by HF-MLFMA and LF-MLFMA with two digits of accuracy, i.e., with a maximum 1% error. In order to achieve this level of accuracy, HF-MLFMA is restricted to a maximum of three levels, but it can be increased to four using LF-MLFMA. Specifically, a bottom-up strategy with 0.25λ lowest-level subdomains is used in HF-MLFMA, whereas a fixed tree structure (but changing subdomain dimensions with respect to frequency) constructed by a top-down strategy is

used in LF-MLFMA. Iterative solutions are also accelerated by a SAI preconditioner constructed from the near-field interactions without filtering. Solutions are performed on the single core of an Intel-Xeon processor with 2.66 GHz clock rate.

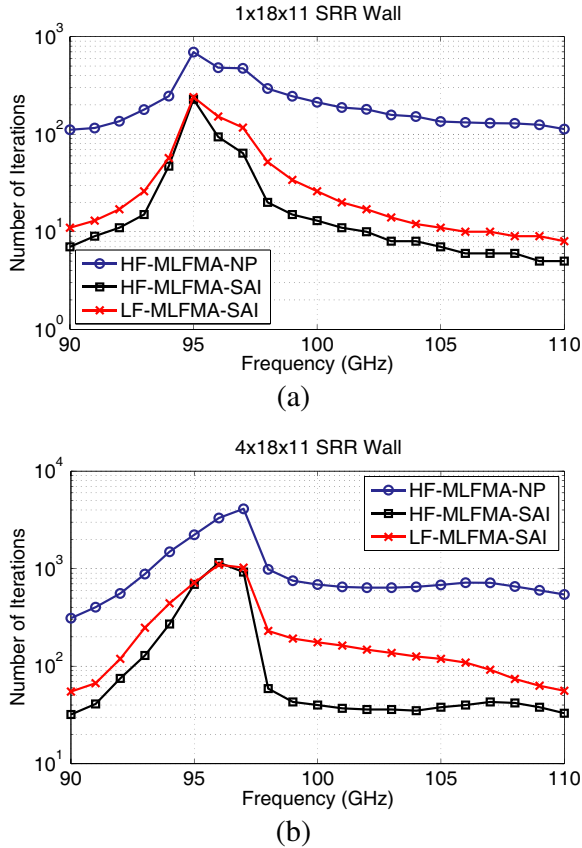


Figure 2. Number of GMRES iterations (for 10^{-3} residual error) required for solving the scattering problems involving (a) one-layer and (b) four-layer SRR walls discretized with 16,236 and 64,944 unknowns, respectively.

Figure 2 presents the number of iterations for 10^{-3} residual error with respect to frequency from 90 GHz to 110 GHz. For the one-layer wall, the number of iterations increases at 95 GHz due to a numerical resonance. The resonance shifts to 97 GHz for the four-layer wall. In fact, as depicted in Fig. 2(b), convergence cannot be achieved at this frequency without preconditioning. We observe that, considering

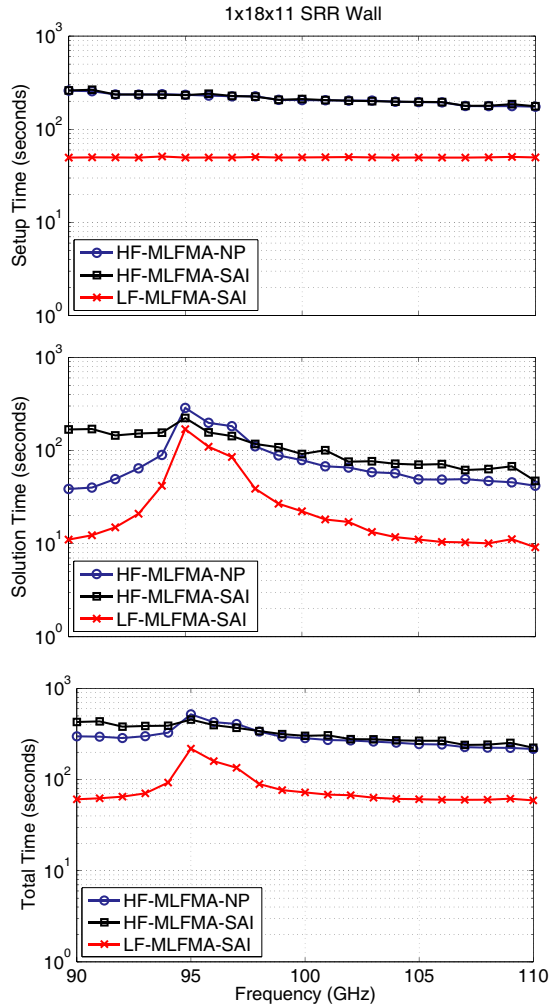


Figure 3. Solutions of scattering problems involving a one-layer SRR wall discretized with 16,236 unknowns. Setup time, solution time, and total time are plotted for frequencies between 90 GHz and 110 GHz.

only HF-MLFMA, the SAI preconditioner reduces the number of iterations significantly, compared to the no-preconditioner (NP) case. However, except for a couple of frequencies around the resonance, using LF-MLFMA increases the number of iterations since the near-field interactions used to construct the preconditioner are fewer in LF-MLFMA, compared to HF-MLFMA. Consequently, Fig. 2 does not show any advantage to using LF-MLFMA rather than HF-MLFMA.

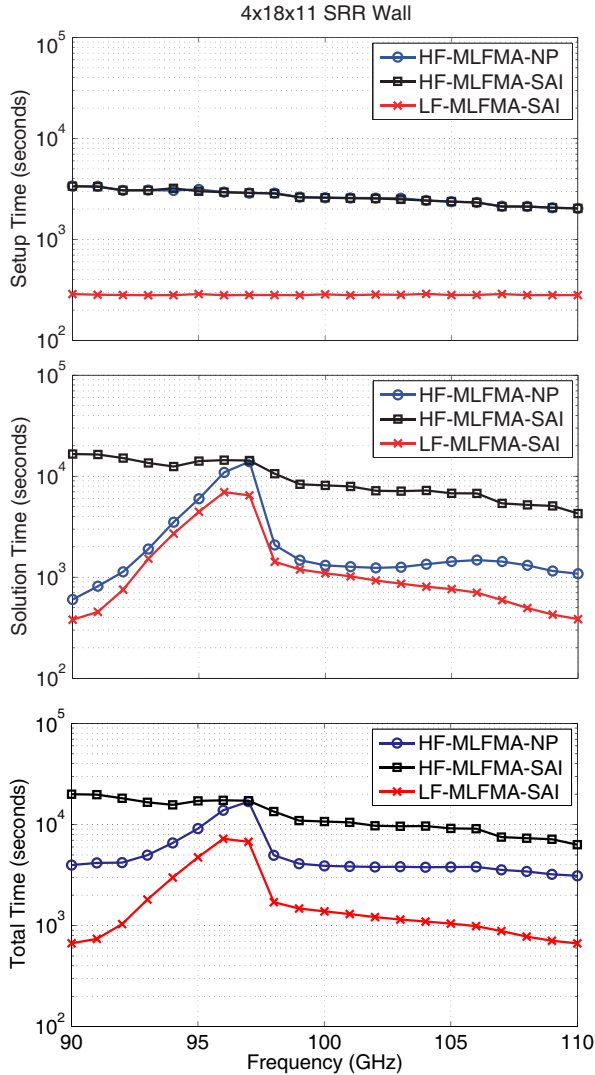


Figure 4. Solutions of scattering problems involving a four-layer SRR wall discretized with 64,944 unknowns. Setup time, solution time, and total time are plotted for frequencies between 90 GHz and 110 GHz.

Figure 3 depicts the setup time, solution time, and total time for the solution of scattering problems involving the one-layer SRR wall. The setup time is dominated by the calculation of near-field interactions, whereas the solution time includes the construction of the SAI preconditioner (if used) and iterations. Fig. 3 shows that

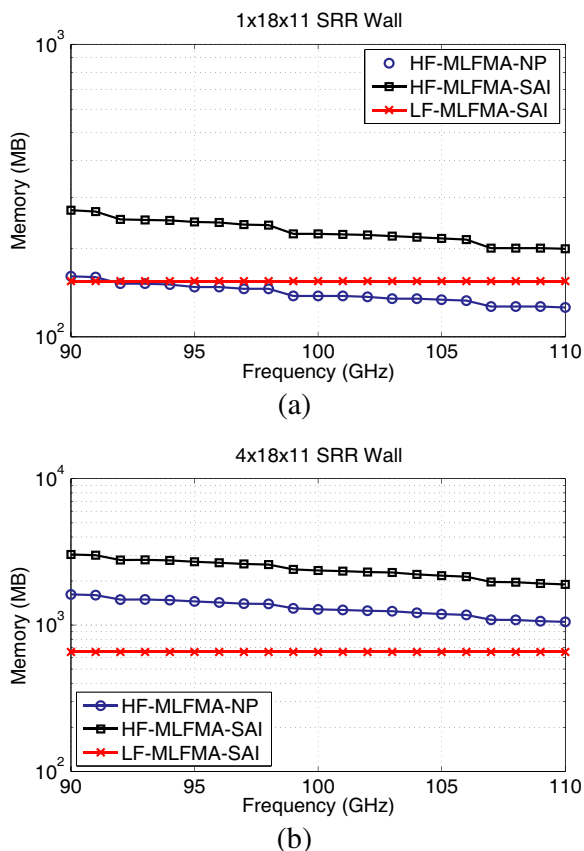


Figure 5. Total memory required for the solution of scattering problems involving (a) one-layer and (b) four-layer SRR walls discretized with 16,236 and 64,944 unknowns, respectively.

the setup time is reduced substantially by using LF-MLFMA, instead of HF-MLFMA. This was expected since the number of near-field interactions is reduced when the number of levels is increased from three to four. Interestingly, as also depicted in Fig. 3, LF-MLFMA also performs better than HF-MLFMA in terms of the solution time. In fact, Fig. 3 demonstrates that the solution time for HF-MLFMA cannot be decreased simply by reducing the number of iterations via the SAI preconditioner because the gain in the iterative-solution time provided by the preconditioner is wasted by additional costs due to its construction. Hence, additional filtering mechanisms are required to optimize the SAI preconditioner and to achieve an acceleration when using HF-MLFMA for metamaterial problems [6]. On the other

hand, using LF-MLFMA always leads to a reasonable number of near-field interactions such that the resulting SAI preconditioner can be constructed efficiently, while the number of iterations can be reduced significantly. The superior performance of LF-MLFMA becomes more apparent in terms of the total time, which includes both setup and solution parts. As presented in Fig. 4, results are very similar for the four-layer SRR wall.

Figure 5 depicts the total memory required for solving metamaterial problems with frequencies from 90 GHz to 110 GHz. Memory required for the MLFMA implementations and the SAI preconditioners are considered without the contribution of the GMRES algorithm. Without preconditioning, memory of HF-MLFMA decreases slowly as a function of frequency from 161 MB to 126 MB for the one-layer wall and 1619 MB to 1051 MB for the four-layer wall. This is because, the size of the lowest-level subdomains in HF-MLFMA is fixed to 0.25λ and the number of near-field interactions decreases with increasing frequency. As illustrated in Fig. 5, using the SAI preconditioner significantly increases the memory requirement. For example, at 90 GHz, the required memory increases to 271 MB and 3037 MB for the one-layer and four-layer walls, respectively. Memory required for LF-MLFMA is almost constant with respect to frequency since the size of the lowest-level subdomains is not restricted to 0.25λ and the same tree structure with four levels is used in the entire frequency range. In other words, the number of near-field interactions is fixed in LF-MLFMA and the memory requirement does not change with small changes in the frequency. Most importantly, we observe that, in addition to faster solutions, LF-MLFMA requires less memory than HF-MLFMA for preconditioned solutions. In fact, for the larger problem, the total memory required for LF-MLFMA with SAI is even less than the memory required for HF-MLFMA without preconditioning.

Finally, we present the solution of scattering problems involving larger metamaterial walls constructed by using $7 \times 19 \times 19$ SRRs. Fig. 6(a) depicts a metamaterial wall, where the SRRs have the same orientation, as usual. In addition to this ordinary wall, we consider another wall involving $7 \times 19 \times 19$ randomly-oriented SRRs, as depicted in Fig. 6(b). Discretizations with the RWG functions on $\lambda/100$ triangles lead to matrix equations involving 207,214 unknowns. The walls are illuminated by a Hertzian dipole located at $x = 1.5$ mm. Two orientations (y direction and z direction) of the dipole are considered for investigating the transmission properties for different polarizations. Problems are solved at 100 GHz with a six-level LF-MLFMA. The ordinary wall in Fig. 6(a) is solved in a total of 3.0 hours on a single-

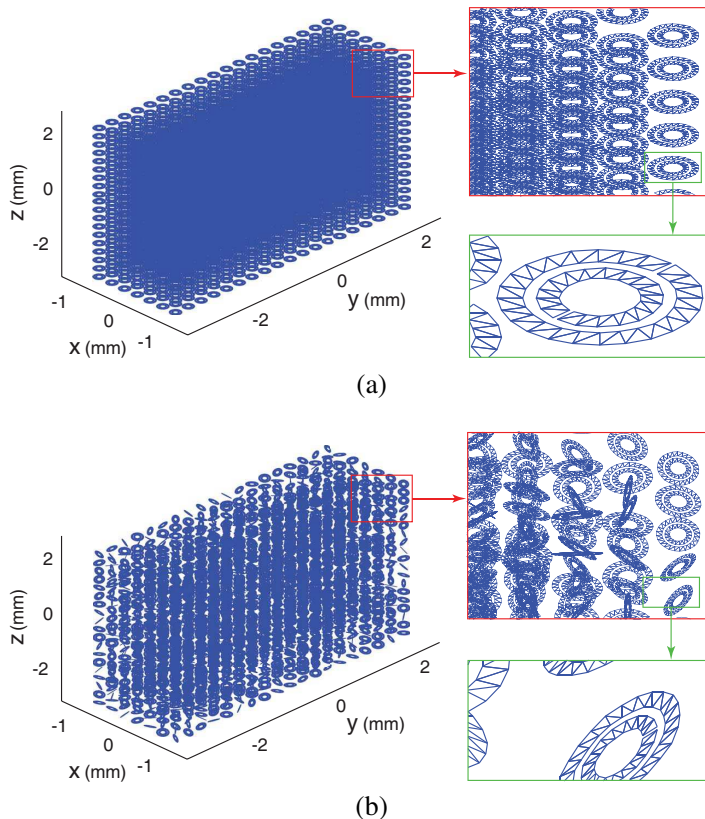


Figure 6. Metamaterial walls involving (a) $7 \times 19 \times 19$ SRRs with the same orientation and (b) $7 \times 19 \times 19$ randomly-oriented SRRs.

core Intel-Xeon processor with 3.6 GHz clock rate. Using the SAI preconditioner, iteration counts are 111 and 108 (for 10^{-3} residual error) when the dipole is oriented in the y direction and the z direction, respectively. The wall in Fig. 6(b) is solved in a total of 3.5 hours, and iteration counts are 145 and 149, respectively.

Figure 7 present the power transmission as a function of location on the $y = 0$ plane for the metamaterial wall in Fig. 6(a). We observe that the shadowing effect occurs only when the Hertzian dipole is oriented in the y direction. For the z orientation, the wall is almost transparent and the power transmission is close to unity in the transmission region on the left of the wall. This is because SRRs do not resonate when the electric field is (almost) perpendicular

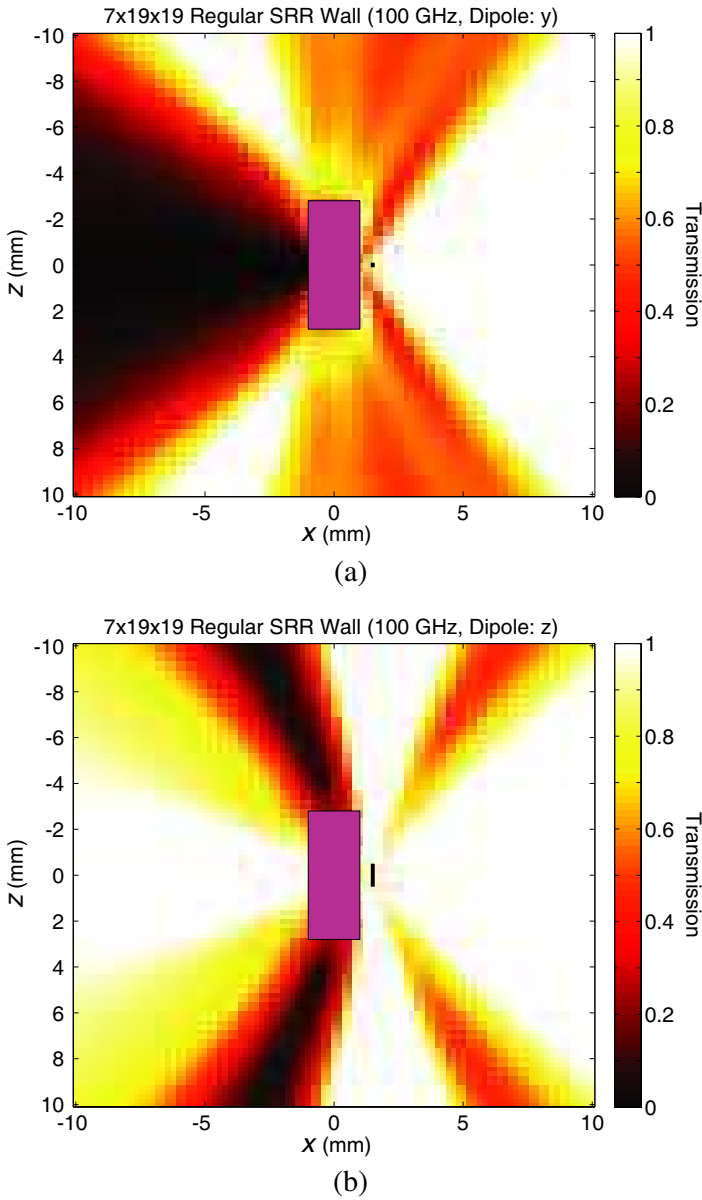


Figure 7. Power transmission as a function of location on the $y = 0$ plane for the metamaterial wall depicted in Fig. 6(a) when the Hertzian dipole is oriented in (a) the y direction and (b) the z direction.

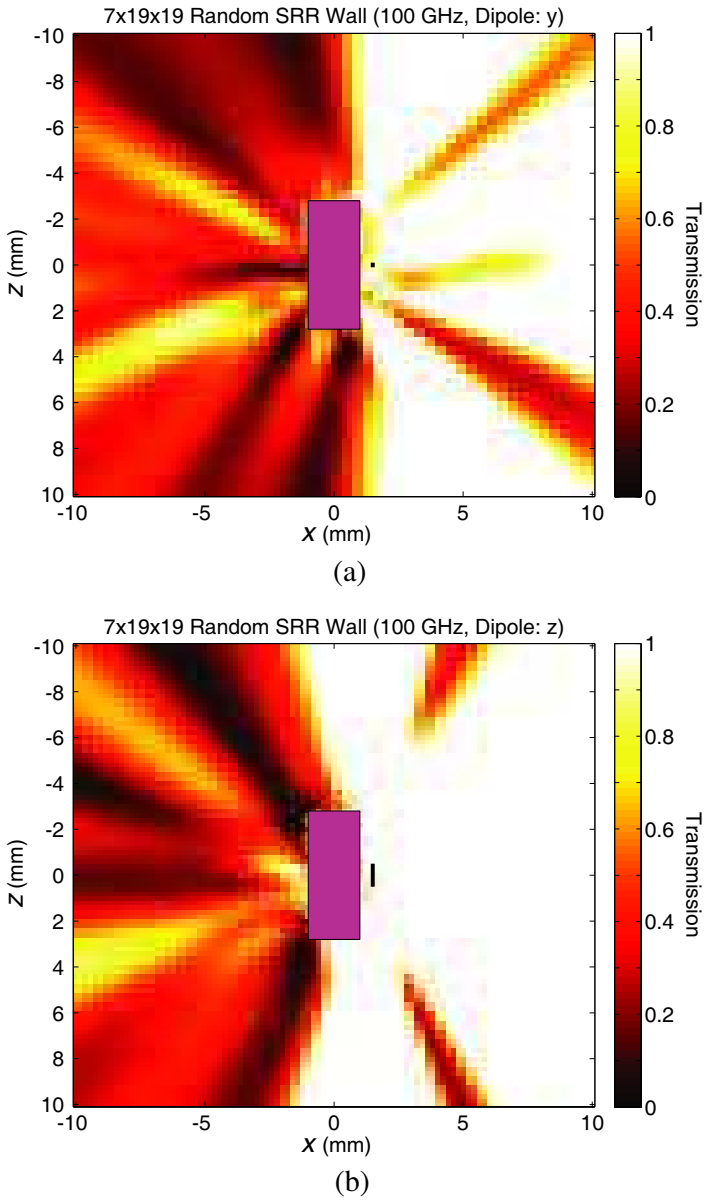


Figure 8. Power transmission as a function of location on the $y = 0$ plane for the metamaterial wall depicted in Fig. 6(b) when the Hertzian dipole is oriented in (a) the y direction and (b) the z direction.

to their surfaces. As depicted in Fig. 8, this major restriction of the metamaterial structures, i.e., the polarization dependency, can be partially eliminated by using randomly-oriented unit cells. Figs. 8(a) and (b) shows that the shadowing effect occurs for both polarizations of the dipole, thanks to the randomly oriented SRRs.

4. CONCLUSION

Metamaterial structures involving small details with respect to the wavelength can be analyzed more efficiently via LF-MLFMA using multipoles, instead of HF-MLFMA using plane waves. We show that accelerated iterative convergence provided by robust preconditioning techniques may not be sufficient to reduce the processing time without overcoming the major bottleneck, i.e., the low-frequency breakdown. An LF-MLFMA implementation accelerated with the SAI preconditioner can provide efficient analysis of realistic metamaterials, such as complicated structures involving randomly-oriented unit cells.

ACKNOWLEDGMENT

This work was supported by the Scientific and Technical Research Council of Turkey (TUBITAK) under Research Grant 107E136, by the Turkish Academy of Sciences in the framework of the Young Scientist Award Program (LG/TUBA-GEBIP/2002-1-12), and by contracts from ASELSAN and SSM. Özgür Ergül was also supported by a Research Starter Grant provided by the Faculty of Science at the University of Strathclyde.

REFERENCES

1. Shelby, R. A., D. R. Smith, and S. Schultz, "Experimental verification of a negative index of refraction," *Science*, Vol. 292, 77–79, Apr. 2001.
2. Eleftheriades, G. V. and K. G. Balmain, *Negative-refraction Metamaterials: Fundamental Principles and Applications*, Wiley-IEEE, New Jersey, 2005.
3. Gokkavas, M., K. Güven, I. Bulu, K. Aydın, R. S. Penciu, M. Kafesaki, C. M. Soukoulis, and E. Özbay, "Experimental demonstration of a left-handed metamaterial operating at 100 GHz," *Phys. Rev. B.*, Vol. 73, No. 19, 193103-1–193103-4, May 2006.

4. Schurig, D., J. J. Mock, B. J. Justice, S. A. Cummer, J. B. Pendry, A. F. Starr, and D. R. Smith, "Metamaterial electromagnetic cloak at microwave frequencies," *Science*, Vol. 314, 977–980, Nov. 2006.
5. Moss, C. D., T. M. Gregorczyk, Y. Zhang, and J. A. Kong, "Numerical studies of left handed metamaterials," *Progress In Electromagnetics Research*, Vol. 35, 315–334, 2002.
6. Gürel, L., Ö. Ergül, A. Ünal, and T. Malas, "Fast and accurate analysis of large metamaterial structures using the multilevel fast multipole algorithm," *Progress In Electromagnetics Research*, Vol. 95, 179–198, 2009.
7. Ylä-Oijala, P., Ö. Ergül, L. Gürel, and M. Taskinen, "Efficient surface integral equation methods for the analysis of complex metamaterial structures," *Proc. European Conf. on Antennas and Propagation (EuCAP)*, 1560–1564, 2009.
8. Ergül, Ö., T. Malas, Ç. Yavuz, A. Ünal, and L. Gürel, "Computational analysis of complicated metamaterial structures using MLFMA and nested preconditioners," *Proc. European Conf. on Antennas and Propagation (EuCAP)*, 2007.
9. Song, J., C.-C. Lu, and W. C. Chew, "Multilevel fast multipole algorithm for electromagnetic scattering by large complex objects," *IEEE Trans. Antennas Propag.*, Vol. 45, No. 10, 1488–1493, Oct. 1997.
10. Chew, W. C., J.-M. Jin, E. Michielssen, and J. Song, *Fast and Efficient Algorithms in Computational Electromagnetics*, Artech House, Boston, MA, 2001.
11. Ergül, Ö., Ç. Yavuz, A. Ünal, and L. Gürel, "Investigation of various metamaterial structures using multilevel fast multipole algorithm," *Proc. IEEE Antennas and Propagation Soc. Int. Symp.*, 1845–1848, 2007.
12. Greengard, L., J. Huang, V. Rokhlin, and S. Wandzura, "Accelerating fast multipole methods for the Helmholtz equation at low frequencies," *IEEE Comput. Sci. Eng.*, Vol. 5, 32–38, Jul.–Sep. 1998.
13. Jiang, L. J. and W. C. Chew, "Low-frequency fast inhomogeneous planewave algorithm (LF-FIPWA)," *Microw. Opt. Technol. Lett.*, Vol. 40, No. 2, 117–122, Jan. 2004.
14. Darve, E. and P. Have, "A fast multipole method for Maxwell equations stable at all frequencies," *Phil. Trans. R. Soc. Lond. A*, Vol. 362, 603–628, Mar. 2004.
15. Wallén, H. and J. Sarvas, "Translation procedures for broadband

- MLFMA,” *Progress In Electromagnetics Research*, Vol. 55, 47–78, 2005.
16. Xuan, L., A. Zhu, R. J. Adams, and S. D. Gedney, “A broadband multilevel fast multipole algorithm,” *Proc. IEEE Antennas and Propagation Soc. Int. Symp.*, 1195–1198, 2004.
 17. Chew, W. C., S. Koc, J. M. Song, C. C. Lu, and E. Michielssen, “A succinct way to diagonalize the translation matrix in three dimensions,” *Microw. Opt. Technol. Lett.*, Vol. 15, No. 3, 144–147, Jun. 1997.
 18. Zhao, J.-S. and W. C. Chew, “Three dimensional multilevel fast multipole algorithm from static to electrodynamic,” *Microw. Opt. Technol. Lett.*, Vol. 26, No. 1, 43–48, Jul. 2000.
 19. Zhao, J.-S. and W. C. Chew, “Applying matrix rotation to the three-dimensional low-frequency multilevel fast multipole algorithm,” *Microw. Opt. Technol. Lett.*, Vol. 26, No. 2, 105–110, Jul. 2000.
 20. Zhao, J.-S. and W. C. Chew, “Applying LF-MLFMA to solve complex PEC structures,” *Microw. Opt. Technol. Lett.*, Vol. 28, No. 3, 155–160, Feb. 2001.
 21. Chu, Y.-H. and W. C. Chew, “A multilevel fast multipole algorithm for electrically small composite structures,” *Microw. Opt. Technol. Lett.*, Vol. 43, No. 3, 202–207, Nov. 2004.
 22. Jiang, L. J. and W. C. Chew, “A mixed-form fast multipole algorithm,” *IEEE Trans. Antennas Propag.*, Vol. 53, No. 12, 4145–4156, Dec. 2005.
 23. Otani, Y. and N. Nishimura, “A periodic FMM for Maxwell’s equations in 3D and its applications to problems related to photonic crystals,” *J. Comput. Phys.*, Vol. 227, No. 9, 4630–4652, Apr. 2008.
 24. Lee, J., J. Zhang, and C.-C. Lu, “Sparse inverse preconditioning of multilevel fast multipole algorithm for hybrid integral equations in electromagnetics,” *IEEE Trans. Antennas and Propagat.*, Vol. 52, No. 9, 2277–2287, Sep. 2004.
 25. Malas, T. and L. Gürel, “Accelerating the multilevel fast multipole algorithm with the sparse-approximate-inverse (SAI) preconditioning,” *SIAM J. Sci. Comput.*, Vol. 31, No. 3, 1968–1984, Mar. 2009.
 26. Koc, S., J. M. Song, and W. C. Chew, “Error analysis for the numerical evaluation of the diagonal forms of the scalar spherical addition theorem,” *SIAM J. Numer. Anal.*, Vol. 36, No. 3, 906–921, 1999.

27. Wu, B.-I., W. Wang, J. Pacheco, X. Chen, T. M. Grzegorzcyk, and J. A. Kong, "A study of using metamaterials as antenna substrate to enhance gain," *Progress In Electromagnetics Research*, Vol. 51, 295–328, 2005.
28. Wongkasem, N., A. Akyurtlu, J. Li, A. Tibolt, Z. Kang, and W. D. Goodhue, "Novel broadband terahertz negative refractive index metamaterials: Analysis and experiment," *Progress In Electromagnetics Research*, Vol. 64, 205–218, 2006.
29. Grzegorzcyk, T. M. and J. A. Kong, "Review of left-handed metamaterials: Evolution from theoretical and numerical studies to potential applications," *Journal of Electromagnetic Waves and Applications*, Vol. 20, No. 14, 2053–2064, 2006.
30. Yu, A., F. Yang, and A. Z. Elsherbeni, "A dual band circularly polarized ring antenna based on composite right and left handed metamaterials," *Progress In Electromagnetics Research*, Vol. 78, 73–81, 2008.
31. Wu, G.-L., W. Mu, X.-W. Dai, and Y.-C. Jiao, "Design of novel dual-band bandpass filter with microstrip meander-loop resonator and csrr dgs," *Progress In Electromagnetics Research*, Vol. 78, 17–24, 2008.
32. Alici, K. B., A. E. Serebrayannikov, and E. Ozbay, "Radiation properties and coupling analysis of a metamaterial based, dual polarization, dual band, multiple split ring resonator antenna," *Journal of Electromagnetic Waves and Applications*, Vol. 24, No. 8–9, 1183–1193, 2010.